JOURNAL OF MATERIALS SCIENCE 23 (1988) 3161–3167

Microstructure and microhardness in alumina gel monoliths

V. SARASWATI
Indira Gandhi Centre for Atomic Research, Kalpakkam 603 102, India

Alumina gel monoliths prepared from aluminium isopropoxide through hydrolysis and chemical polymerization are porous, transparent, and consist of ultrafine particles. The monolithic xerogels exhibit lamellar, cellular and fractal microstructures which are found to arise due to instabilities during drying. Phase separation can occur during ageing and drying and influence the microstructure. The Vickers indentation hardness shows a power-law dependence on relative density.

1. Introduction

In recent years gel-processed materials have evoked considerable interest in the preparation of oxide ceramics and glasses. Monolithic gels can be produced by hydrolysis, condensation and polymerization of metal alkoxides which on heating at a low temperature leave behind an oxide network [1, 2]. The significance of the chemical polymerization route is that monolithic bulk pieces, fibres or films can be produced from single or multicomponent oxides, which is not possible by the conventional sol–gel method. The structural evolution of a transparent boehmite xerogel and the opitical absorption properties of doped and undoped monoliths have been studied earlier [2, 3]. Disorder in the properties of transition aluminas and lamellar microstructures were observed in the monoliths. the evolution of microstructure on dehydration and its influence on microhardness is reported here. The fractal and cellular microstructures now observed owe their origin to the phase instabilities arising from flow displacements during drying. The microhardness is influenced by the microstructure and instabilities. In the monoliths the microhardness follows a power-law dependence on relative density similar to that of cellular materials. Cellular ceramics can have wide applications as they are light and stiff [4].

2. Experimental details

The gels were prepared from aluminium isopropoxide following the hot hydrolysis method described by Yoldas [1]. The alkoxide, water and catalysing hydrochloric acid were in the molar ratios 1 : 100 : 0 3. A transition-metal powder was added to the sol and after ageing a clear coloured concentrated sol was set aside for gelation and drying in flat dishes. The iron-doped alumina xerogel was yellow, chromium-doped green, and the copper-doped was green or blue depending on the concentration and chlorine content. The dopant concentration determined by spectrochemical analysis was low (< 1 wt %) and did not influence the X-ray diffraction or infrared spectra. As the porous gels are reactive, the transition-metal ions bind to the surface as an aquochlorocomplex [5] in the xerogel and penetrate into the matrix on heating. It has been observed [6] that Fe^{3+} and Cr^{3+} have a good solubility and Cu^{2+} to some extent [7] in the alumina matrix. This has been confirmed from visible-range optical absorption measurements [5].

The polymorphic transitions of both doped and undoped boehmite gels occur approximately as

$$\text{boehmite (AlOOH)} \xrightarrow{350^\circ C} \gamma\text{-}Al_2O_3$$

$$\xrightarrow{950^\circ C} \delta\text{-}Al_2O_3 \xrightarrow{1200^\circ C} \alpha\text{-}Al_2O_3$$

TABLE I Hardness and density changes with heat treatment

Heating temperature (°C)	Material*	Density ($g\,cm^{-3}$)	Hardness (load 100 g) ($kg\,mm^{-2}$)
26 to 100	AlOOH (with or without dopant)	1.65 ± 0.05	17.7 ± 0.2 (25 g)
400 to 800 (duration and temperature variable)	$Al_2O_3 \cdot xH_2O \cdot R_mO_n$	1.37 ± 0.05	55 ± 6, 116 ± 6
900 to 1000 (4 h to 3 days)	$Al_2O_3 + R_mO_n$	1.51 ± 0.05	144 ± 6, 177 ± 6
1150, 40 h	$Al_2O_3 + R_mO_n$	2.17 ± 0.05	343 ± 8
1300, 12 h	$Al_2O_3 + R_mO_n$	2.7 ± 0.05	628
1500, 90 h	$Al_2O_3 + R_mO_n$	3.08 ± 0.05	907

*R stands for Cu, Cr or Fe with concentration less than 1 wt %. The nature of the binding oxide depends on the heat treatment.

0022–2461/88 $03.00 + .12

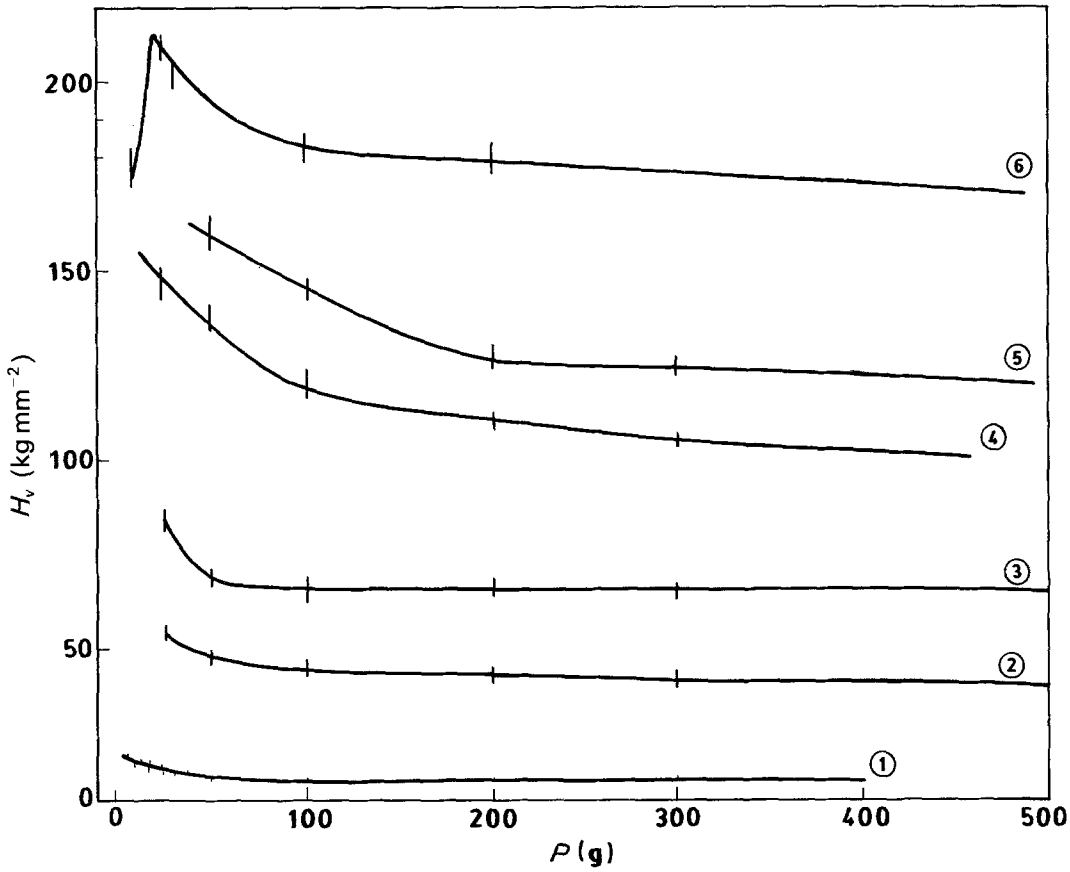

Figure 1 Hardness against load in alumina monoliths: (1) boehmite, (2) copper-doped γ phase, (3) copper-doped δ phase, (4) chromium-doped γ phase, (5) undoped γ phase, (6) chromium-doped δ phase.

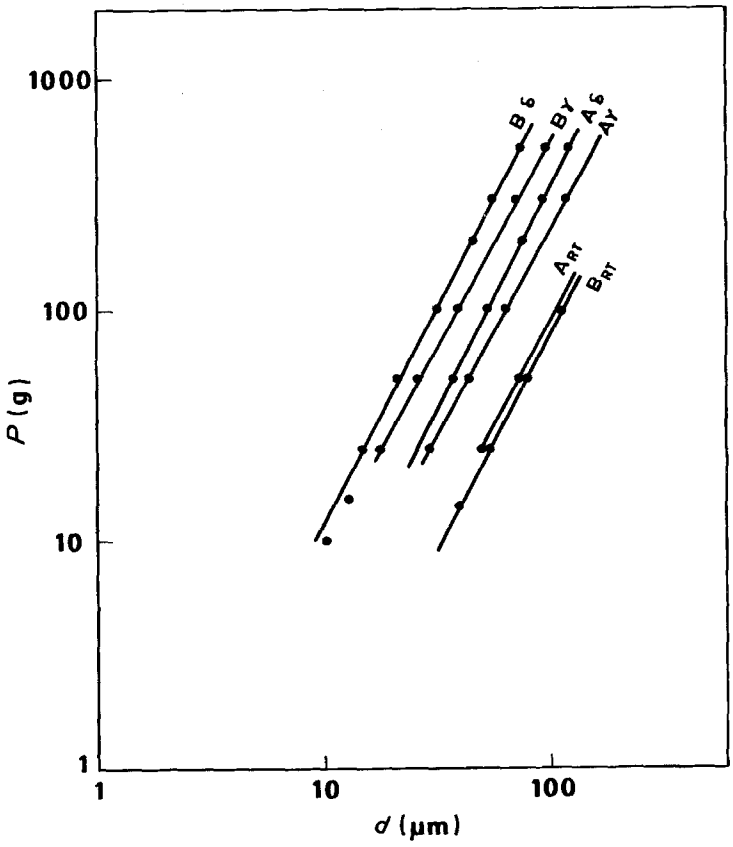

Figure 2 Plot of load against diagonal in two batches of gel, A and B. RT = Room temperature.

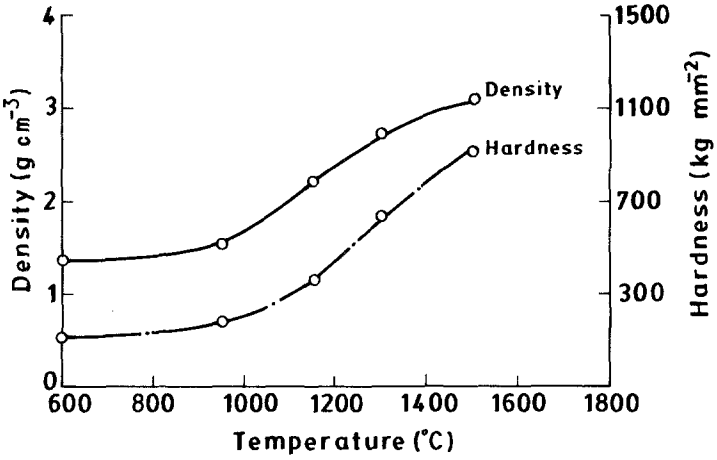

Figure 3 Microhardness and density change against temperature.

There is a spread in transition temperatures depending on the duration of hold at a temperature.

The optical transmission properties were good and the absorption in the visible range reflected the coordination and valence state of the dopant transition-metal ion [5]. The gel monoliths retained transparency up to 1000° C and the opitical transmission improved with heating. They became opaque on heating above 1000° C. The optical and structural properties and their changes have been described in detail in earlier work [2, 3]. The xerogels were porous and densification set in rapidly above 1100° C. Transmission electron microscopy, surface area and pore size distribution measurements showed the average particle size as 8 nm and the pore size 3 nm for boehmite.

The Vickers microhardness numbers, H_v, were measured with a Leitz miniload tester. As the xerogel had a natural gloss no grinding or polishing of the surface was needed for observing the indentation. The gloss was lost on heating above 1200° C. The material was then polished with a fine diamond paste. The microhardness of boehmite xerogel was low at 17 kg mm^{-2}. For the low concentration used the nature of the dopant and its concentration did not have much influence on the hardness value. It was, however, influenced by the hydrolysing conditions owing to the change in crosslinking and connectivity on polymerization. The variations of hardness with load and temperature of dehydration are shown in Fig. 1. The hardness values and densities are shown in Table 1. The load dependence of the impression diagonal is shown in Fig. 2, and Fig. 3 shows the variation of microhardness with density. It deserves mention that the indentation marks were clear in spite of the porosity, essentially because of the fine sizes of the pores. The microhardness increases for smaller loads, when the impression diagonal is comparable to the lamellar width. The impression diagonal in all monoliths from boehmite to the alpha phase exhibited crack-free square impressions at 500 g load, whereas pressed pellets of conventional alumina show microcracks even at 200 g load.

3. Results and discussion

3.1. Microstructure

The fractured surfaces of all gel monoliths exhibited

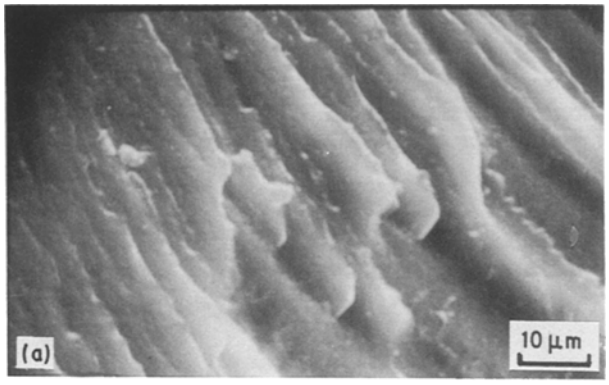

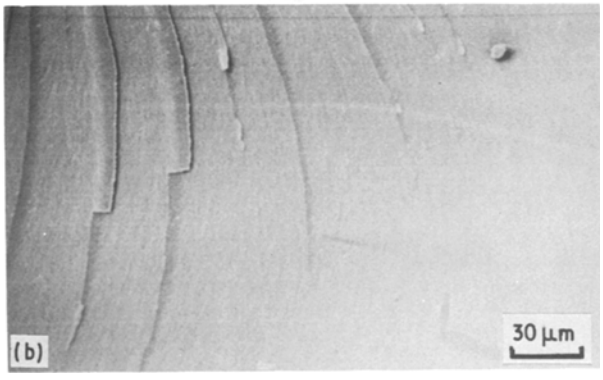

Figure 4 Fractured surfaces of (a) copper doped γ-Al_2O_3, (b) slip steps in the boehmite phase, (c) colony structure in δ-Al_2O_3.

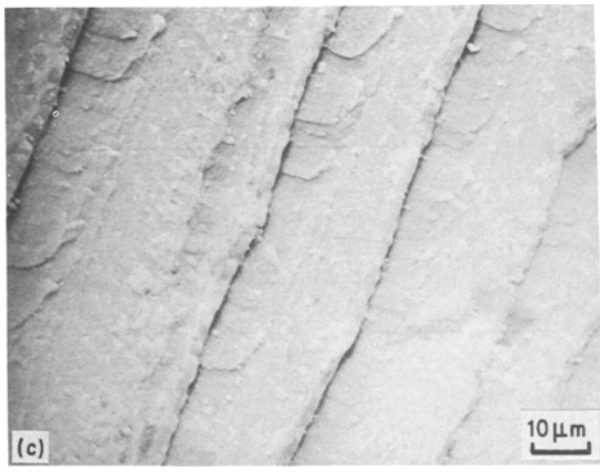

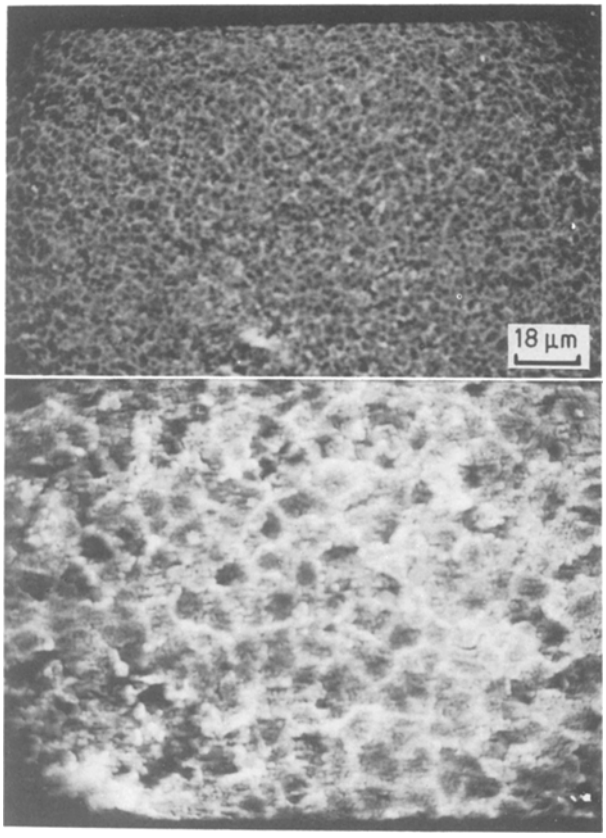

Figure 5 Cellular microstructure in copper-doped gel in the α phase.

layer-like structures (Fig. 4) with patterns similar to what is called a colony structure. The monoliths in the α phase showed grain formation. Cellular microstructures were observed in some monoliths. Fig. 5 shows the microstructure in a sintered copper-doped monolith in the α-alumina phase. The average cell size is 3.2 μm. The grains at the cell walls are bigger (0.8 μm) compared to the inner region (0.3 μm). The colony structure is a superposition of cellular and lamellar structure [8]. This structure is said to arise when an impurity or excess of one constituent diffuses much faster ahead of the interface. This causes the development of cell structure due to instability and constitutional supercooling [8]. Since the doped and undoped gels show similar patterns the cell formation cannot be ascribed to the dopant as impurity. Instead, it can be attributed to a viscosity difference, The solidifying gel can be considered as a two-fluid system of differing viscosities, the polymeric gel and water. As gelation progresses, water is displaced by the more viscous gel. It is similar to a Hele Shaw cell and the complex microstructure is fractal [9].

Fig. 6 shows a micrograph of ion-doped alumina in the γ phase. Self-similarity was demonstrated from micrographs at different magnifications. Several lines were chose for measurements. The number of steps required to traverse a line was plotted against the step size on a logarithmic scale for a few lines. The slope, which gives the fractal dimension, was 1.12 ± 0.01. A line fractal is related to a surface fractal as $D_S = D_L + 1 = 2.12$ [10]. The surface is thus a smooth fractal. Materials with layered structure, fine-size particles and micropores are seen to show smooth fractals [11]. The xerogels described here have nanometre-size particles and micropores of size 3 nm. They also have a layered structure. Hence a smooth fractal is to be expected.

Solute segregation or its periodic distribution is implicit in the cell development. Fluctuations in density could be anticipated as observed by Tanaka *et al.* [12] in organic polymers. In the inorganic system phase separation as a function of temperature was

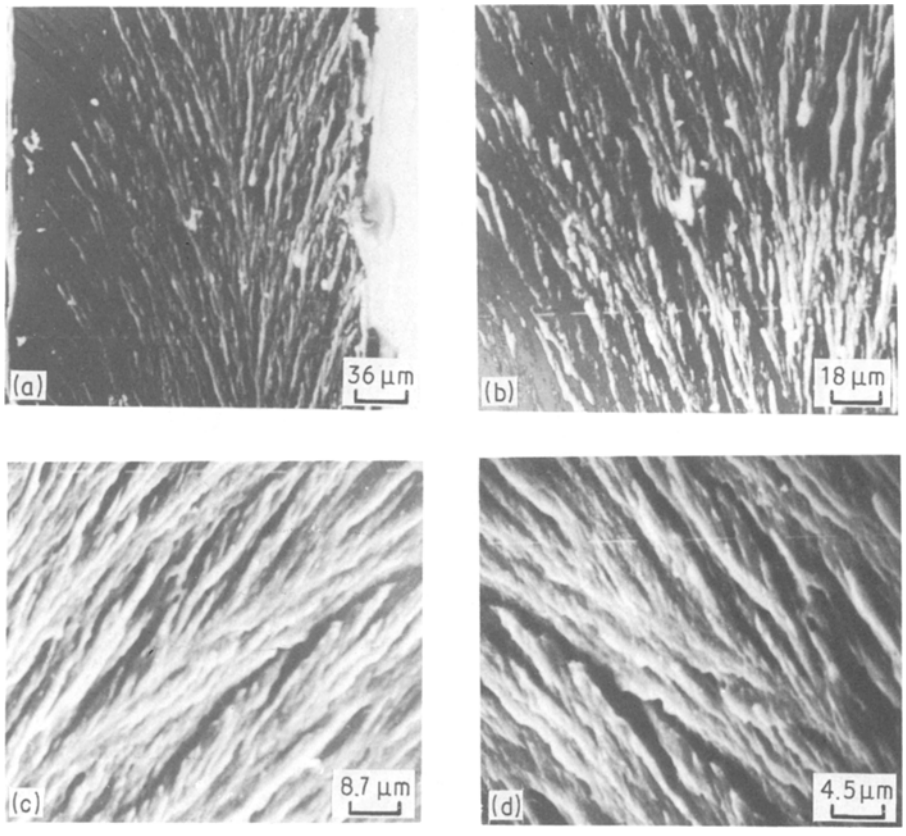

Figure 6(a–d) Microstructure in iron-doped γ-Al_2O_3 at different magnifications. (c) and (d) are with stage tilt.

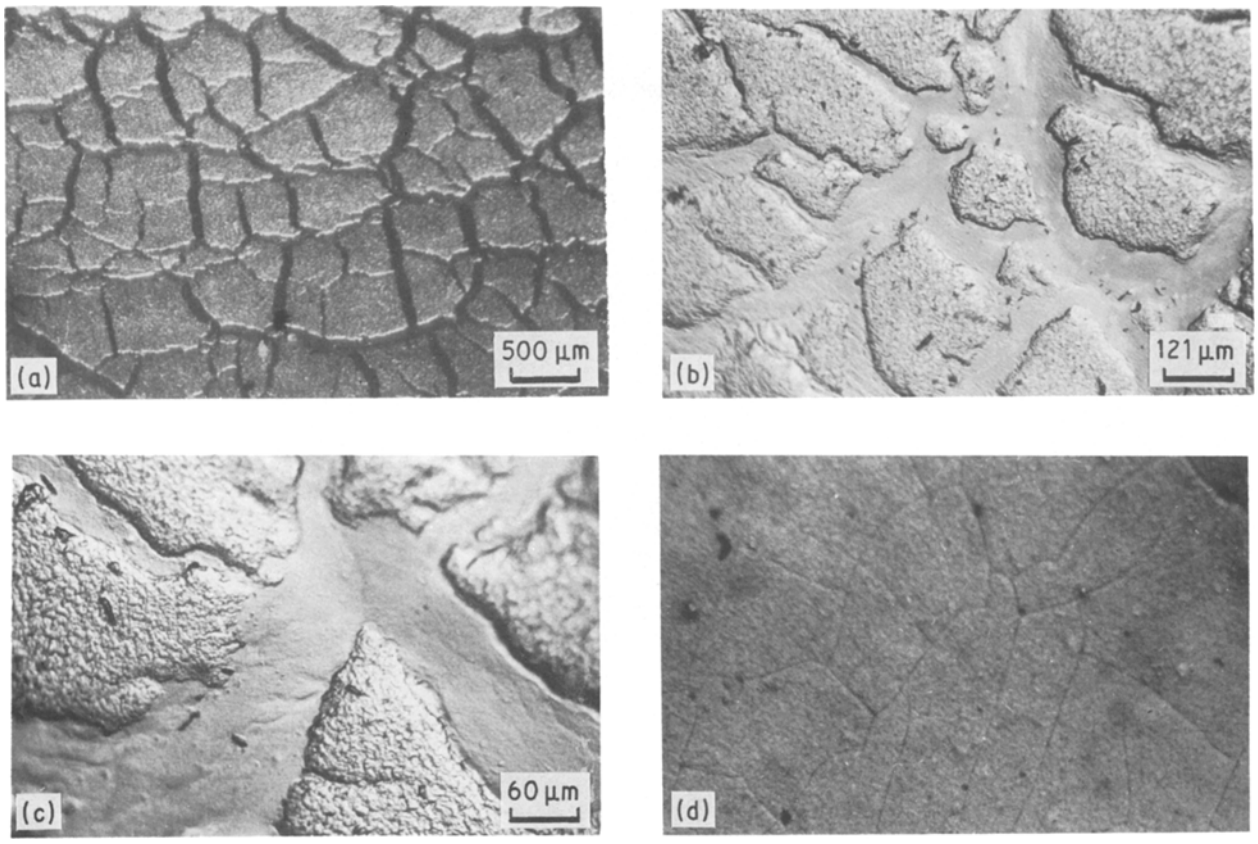

Figure 7 Phase separation in chromium-doped monoliths, top surface, (a–c) different magnifications of boehmite phase; (d) after heat treatment at 1150° C for 40 h

observed in metal alkoxide gels consisting of monomers, linear polymers and branched polymers [13]. Partlow and Yoldas [14] found that titania gels shrank by expelling the solvent. We have observed microstructures indicating density fluctuation in some copper-doped alumina gels [2]. Phase separation on the surface of the doped xerogels is noticeable, especially when the sols are set to dehydrate at a high concentration. For lower-concentration sols the dry xerogel surface is smooth and defect-free. Fig. 7 shows the separation into polymeric and particulate regions in a chromium-doped alumina gel. Further evidence of phase separation is the growth of γ-alumina whiskers from a copper-doped boehmite gel. Crystalline γ-alumina whiskers [15] grew out of the gel solution and also on ageing a monolithic gel (Fig. 8). Though α-alumina whiskers are common, this is probably the first report of crystalline γ-alumina whiskers grown at room temperature. To summarize, during the drying of the monolith, instability and phase separation influence the microstructural changes significantly.

3.2. Microhardness

The microhardness of boehmite xerogel is low, 17 kg mm^{-2}, similar to an organic polymer like nylon. With the heating of xerogel the indentation hardness increases due to one or more of the following reasons: (i) removal of adsorbed water with heating, (ii) rearrangement of oxygen atoms as polymorphic transitions occur which might also involve changes in bond character, and (iii) pore volume reduction accompanied by densification.

In the γ phase the increase in H_v is almost 10 times (Table I) and is due to the loss of water and rearrangement of oxygen to form alumina. X-ray diffraction studies have shown that the γ phase has a cubic close-packed arrangement of oxygen which rearranges to a hexagonal form on heating above 1150° C. The change in crystalline density due to these structural transformations is low (3.65 g cm^{-3} for γ compared to 3.97 g cm^{-3} for α) and their contribution to the microhardness is negligible. Pore volume reduction takes place above 1000° C and the density increases sharply as a hexagonal corundum phase appears. H_v follows

TABLE II Vickers hardness and relative density

Gel material	Density (g cm^{-3})	ϱ/ϱ_0	H_v(exptl) (kg mm^{-2})	$H_0(\varrho/\varrho_0)$ (kg mm^{-2})*	$H_0(\varrho/\varrho_0)^2$ (kg mm^{-2})*
γ-alumina	1.37 ± 0.03	0.345	116 ±4	552	190
δ-alumina	1.51 ± 0.03	0.38	144 – 177	608	231
α-alumina					
1150° C/40 h	2.17 ± 0.03	0.547	343 ± 10	875	478
1300° C/12 h	2.7 ± 0.03	0.68	628 ± 10	1088	739
1500° C/90 h	3.08 ± 0.03	0.776	904 ± 20	1241	963

*ϱ_0 = 3.97 g cm^{-3} and H_0 = 1600 kg mm^{-2} as for corundum.

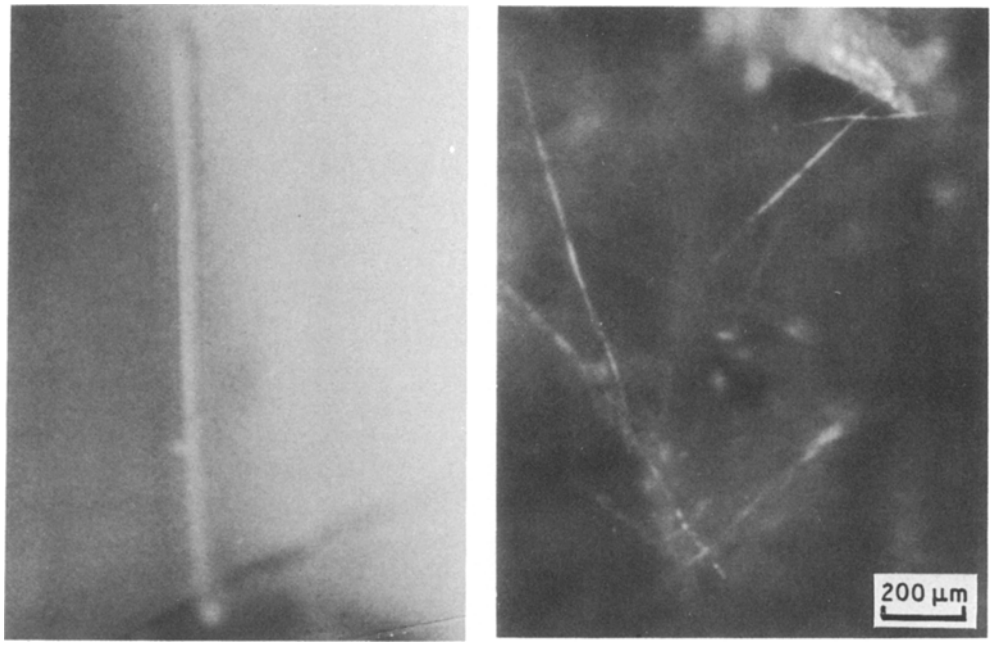

Figure 8 Growth of γ-alumina whiskers on ageing in copper-doped monolith.

the changes in density as can be seen from Fig. 3. In Table II the experimental measurements are compared with values expected from the density. The hardness value plotted against relative density ϱ/ϱ_0 on a log–log scale shows a slope of 2.4 (Fig. 9). Ashby [4] has discussed the deformation mechanisms possible for materials with cellular structure. As the cell walls are capable of bending and buckling, cellular materials are compressible under load. Hence, because they yield plastically, the indentation hardness is lower than that of a dense solid. The indentation hardness for an open cell structure with relative density less than 0.3 was calculated to be proportional to $(\varrho/\varrho_0)^{1.5}$ where ϱ is the density of the gel and ϱ_0 the crystalline density. Mackenzie and Shuttleworth [16] found the bulk and shear moduli for porous solids to be proportional to the square of relative density in the range 0.8 to 1.0. The relative densities in our xerogels are in the range 0.3 to 0.8 and the slope is higher at 2.4.

As mentioned above, the impression diagonals were good and devoid of cracks in spite of the porosity, even at 500 g load. This is due to the flawless nature of the specimen and the absence of microcracks when it is prepared from nanophase particles. The material could be tough although the hardness may be lower. Breval *et al.* [17] noticed a similar absence of radial cracking in nickel-dispersed alumina gels.

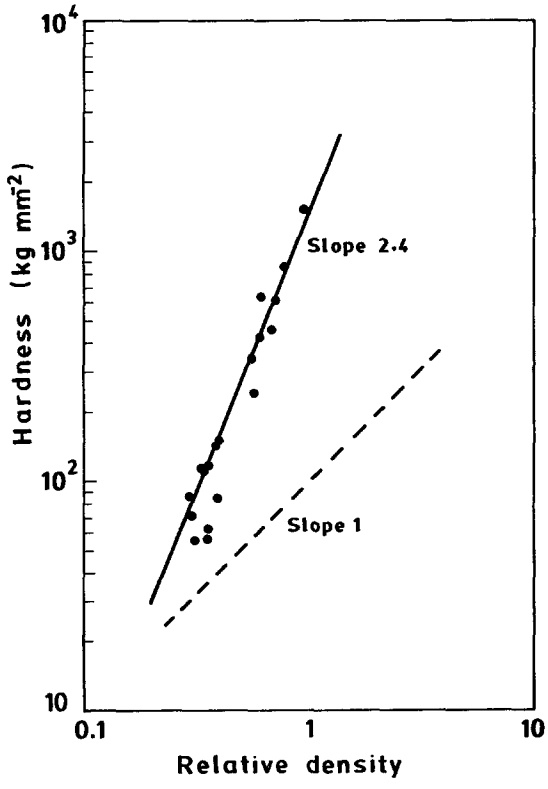

Figure 9 Hardness against relative density plot. All doped and undoped monoliths are included.

4. Conclusions

The microstructure observed in all xerogels was a combination of cellular and lamellar microstructures. These are fractals. The dehydration in a flat dish and displacement of water through the porous gel are considered to be responsible for these patterns. The microhardness evolves with heat treatment of the xerogels due to the removal of adsorbed water and structural rearrangements. The cellular microstructure seems to exert the dominant influence on the indentation hardness, which is related to the density by a power law.

References

1. B. E. YOLDAS, *Amer. Ceram Soc. Bull.* **54** (1975) 289.
2. V. SARASWATI, G. V. RAO and G. V. RAMARAO, *J. Mater. Sci.* **22** (1987) 2529.
3. V. SARASWATI and G. V. RAMARAO, *J. Mater. Sci. Lett.* **5** (1986) 1095.
4. M. F. ASHBY, *Met. Trans.* **14A** (1983) 1755.
5. V. SARASWATI and G. V. RAMARAO, *Bull. Mater. Sci.* **9** (1987) 193.
6. G. T. POTT and B. D. McNICOL, in "Surface Chemisty of Oxides" (Faraday Society, London, 1971) p. 121.
7. J. C. SUMMERS and R. L. KLIMICH, in "Catalysis", Vol. I, Edited by J. W. Hightower (North-Holland, Amsterdam, 1973) p. 293.
8. B. CHALMERS, "Principles of solidification" (Wiley,

New York, 1964) p. 152.
9. J. NITTMAN, G. DACCORD and H. E. STANLEY, in "Fractals in Physics", edited by L. Pietronero and Tossatti (Elsevier, 1986) p. 193.
10. B. B. MANDELBROT "Fractal geometry of nature" (Freeman, San Francisco, 1982).
11. D. FARIN, S. PELEG, D. YAVIN and D. AVNIR, *Langmuir* **1** (1985) 397.
12. T. TANAKA, S. T. SUN, T. HIROKAWA, S. KATAYAMA, J. KUCERA, Y. HIROSE and T. AMIYA, *Nature* **325** (1987) 796.
13. D. W. SCHAEFER and K. D. KEEFER, in "Better Ceramics through Chemisty", edited by. C. J. Brinker, D. R. Ulrich and D. E. Clark (Elsevier/North-Holland, New York, 1984) p. 1.
14. D. P. PARTLOW and B. E. YOLDAS, *J. Non-Cryst. Solids* **46** (1981) 153.
15. V. SARASWATI and G. V. N. RAO, *J. Cryst. Growth* **83** (1987) 606.
16. J. K. MACKENZIE and R. SHUTTLEWORTH, *Proc. Phys. Soc.* **62** (1949) 833.
17. E. BREVAL, G. C. DODDS and N. H. McMILLAN, *Mater. Res. Bull.* **20** (1985) 413.

Received 30 July 1987
and accepted 27 January 1988